Low-temperature anomalous spin correlations and Kondo effect in ferromagnetic SrRuO_{3}/LaNiO_{3}/La_{0.7}Sr_{0.3}MnO_{3} trilayers

Sayandeep Ghosh, R. G. Tanguturi, P. Pramanik, D. C. Joshi, P. K. Mishra, S. Das, and S. Thota

Phys. Rev. B **99**, 115135 — Published 25 March 2019

DOI: 10.1103/PhysRevB.99.115135

Low-temperature Anomalous Spin Correlations and Kondo Effect in Ferromagnetic $SrRuO_3/LaNiO_3/La_{0.7}Sr_{0.3}MnO_3$ Trilayers

Sayandeep Ghosh,[1] R. G. Tanguturi,[1] P. Pramanik,[1] D. C. Joshi,[1] P. K. Mishra,[1,*] S. Das,[2,†] and S. Thota[1,‡]

[1] *Department of Physics, Indian Institute of Technology Guwahati, Assam, 781309, India.*
[2] *Department of Materials Science and Engineering, University of California, Berkeley, 94720, USA.*

(Dated: March 12, 2019)

A systematic comparative study of the electronic transport and ferromagnetic resonance of ultrathin trilayers (TLs) of $SrRuO_3/LaNiO_3/$ $La_{0.7}Sr_{0.3}MnO_3$ on (001)- and (111)-oriented $SrTiO_3$ (STO) substrates has been reported. An unusual upturn in resistivity $\rho(T)$ at low-temperature (so called Kondo-like behaviour) accompanied by the negative magneto-resistance has been observed. For temperatures larger than the Kondo temperature (T_K), $\rho(T)$ is in good agreement with the Hamann's impurity resistivity model $\rho(T>T_K) \propto (ln(T/T_K))^{-2}$ for spin S=1/2 and 3/2 for the TLs on (001)-STO and (111)-STO, respectively. At the temperatures $T \gg T_K$, electron-electron ($\rho(T) \propto T^2$) contribution dominates over those appearing due to the electron-phonon interaction ($\rho(T) \propto T^5$) and 2-Magnon scattering. Using the ferromagnetic resonance near the Curie temperature of $La_{0.7}Sr_{0.3}MnO_3$, we evaluated the contribution of surface anisotropies (K_s) as well as in-plane volume anisotropies (K_ν) : $K_s \sim -9.57 \times 10^{-4}$ J/m^2 (-6.68 $\times 10^{-4}$ J/m^2) and $K_\nu \sim 4.04 \times 10^5$ J/m^3 (3.31×10^5 J/m^3) for the TLs on (001)-STO (TLs on (111)-STO). In addition, the Gilbert damping constant is determined which varies between 0.32 (0.23) and 0.16 (0.19) having spin mixing conductance, $g^{\uparrow\downarrow} = 5.2 \times 10^{19} m^{-2}$ ($13.38 \times 10^{19} m^{-2}$) for TLs on (001)-STO ((111)-STO).

I. INTRODUCTION

Ultrathin multilayers of perovskite oxides are quite widely investigated material in the scientific community because they give rise to unusual physical phenomena across the interfaces due to the electronic reconstruction[1–5]. Such interesting properties of strongly correlated oxides have drawn immense attention for the production of promising electronic devices such as spintronics devices, sensing devices etc[6–9]. Particularly, multilayers of transition metal oxides based perovskites have shown a variety of fascinating physical properties across the interfaces such as high-mobility electron gas and superconducting behaviour, colossal magneto-resistance (CMR), ferroelectricity, etc[10–16]. Among these properties, CMR behaviour was observed in the doped manganites family around their ferromagnetic Curie temperature (T_C)[17]. Generally, thin films exhibit markedly different features from their bulk counterpart due to the dominance of surface effects, substrate induced strain and/or oxygen deficiency[18]. Apart from the difference in the mechanical behaviour their electronic properties such as metal-to-insulator transitions are also more prominent in the 2D structures[19–23].

In recent years, research on interfaces of ferromagnetic (FM) $LaSrMnO_3$ (LSMO) and $SrRuO_3$ (SRO) layers has attracted much attention because of the artificially induced antiferromagnetic coupling across the interface[24,25]. Unlike manganites, $LaNiO_3$ (LNO) is another interesting perovskite material which exhibits metallic behaviour with paramagnetic property[26–28]. Combination of such metallic-paramagnet with highly anisotropic ferromagnets like SRO or half-metallic ferromagnets such as LSMO has drawn attention recently due to their enhanced magnetic response including exchange-bias[29–36]. Among the LNO based multilayer systems LSMO/LNO heterostructures display the orbital reorientation induced by the charge transfer from Mn^{3+} to Ni^{3+}, across the interfaces[37]. Such multilayers exhibit very large magnetic frustration, spin-glass behaviour, and the intriguing exchange bias effect at the interfaces[37]. Additionally, charge transfer mechanism and interfacial magnetism also observed in $(LaNiO_3)_n/(LaMnO_3)_2$ superlattices with $2 \leq n \leq 5$ unit cells grown on (001) TiO_2-terminated $SrTiO_3$ (STO) single-crystal substrates[38].

Interface plays an important role to induce the electronic as well as magnetic transport properties of the heterostructures. Sánchez *et. al.* experimentally investigated the exchange-bias effect (H_{EB}) and enhanced coercivity (H_C) in $La_{0.75}Sr_{0.25}MnO_3$ (60 nm)/$LaNiO_3$ (30 nm) multilayers grown on (001) oriented STO single crystal substrate[39]. These authors concluded that variation in the oxidation states of Ni and Mn across the interfaces of LSMO and LNO was responsible for such unexpected observations of H_{EB} and H_C which vanishes around $T = 50$ K[39]. Gibert *et. al.* observed similar type of results in the case of LNO-$LaMnO_3$ (ferromagnet with $T_C \sim 200$K) heterostructures grown on (111) oriented STO substrate[40].

Like magnetic properties, electronic transport properties of perovskite thin films strongly depend on the micro structures and substrate induced strain. Strain induced anisotropic magneto-resistance (MR) play a major role in deciding over the suitability of the heterostructures, while fabrication of many devices[41]. As compared to the anisotropic behaviour of manganite, SRO thin films

* pankaj.mishra@iitg.ernet.in
† sujitdas@berkeley.edu
‡ subhasht@iitg.ernet.in

and their heterostructres exhibit giant anisotropy in both magnetic as well as in MR[42–44]. Generally, the electrical resistivity exhibits anisotropic behaviour at low temperatures depending whether the applied magnetic-field is along or perpendicular to the plane of the SRO films. In general, observed anomalous change in the resistivity at low-temperatures strongly depends on the microstructure defects. This feature is directly related to the strongly correlated electronic structure[45]. Moreover, lowering the dimensionality of the heterostructured LNO layer, Liu *et. al.* found an enhancement in electron-electron correlations with strong Mott-type metal-to-insulator transition with the latent competing state of charge ordering in quantum confined ultrathin superlattices of LNO/$LaAlO_3$ (LAO)[46]. Redistribution of ligand hole density and reduction of Ni-O-Al covalence in the LNO-LAO superlattices results such exotic phenomena which are confirmed by the *ab initio* cluster calculations[46].

Best of our knowledge we find that in the literature that there are few reports discussing about the electronic transport mainly arises due to the inelastic scattering in SRO thin films which is associated to the directly bound to the delocalized state as temperature is raised[43–51]. It has been argued that the scattering observed at low temperature can be explained by incorporating the quantum correrctions which may be of 2D or 3D limit depending on the nature of the charge carriers[49,52]. Furthermore, mono-layer SRO thin films exhibit the MR behaviour with negative sign and follow square dependence on the magnetic field indicating the theory in 3D limit associated with MR drops at high magnetic fields[48].

On the other hand, the low temperature resistivity of manganite thin films were explained by the electron-electron interaction and weak localization effects. Matritato *et. al.* reported the Kondo like spin dependent transport behaviour in LSMO thin films and found that transport depends mainly on the layer thickness[53]. In addition Kondo behaviour also depends quite significantly on the direction of the applied magnetic field since the spin states (s_z) of the easy axis is generally greater than one (s >1). However, it is difficult to identify the spin flipping phenomena encountered by the conduction electrons when they interact with the magnetic impurity[54]. Although there is no direct visualization of the weak localization effects in manganite thin films, it could be detected by applying strong magnetic field. This way one can also probe the weak localization and their individual contributions including the interaction term. Quantum correction of the transport behaviour was also reported in manganite thin films[55,56].

Since last few decades 2D perovskite materials have played major role in bringing a significant advancement in proposing a state-of-art technology for energy storage devices due to their superior electronic and optoelectronic behaviour[57–59]. These perovskite materials (LSMO/SRO superlattices) have also been demonstrated as a promising candidate for an alternative room-temperature magnetic refrigerators at very small scales, as they have better magnetocaloric effect and cooling power[60]. In addition owing to their bipolar resistive switching memory effect and inverted hysteresis with giant exchange bias these superlattices can be a major component for the storage device [61,62]. Apart from their superior optoelectronic features these materials exhibit better thermal response. As the heat current is passed perpendicular to these superlattices, it was observed that they show transverse thermoelectric effect in the presence of external magnetic field [63]. In the context of the trilayers there are few works that have explored their magneto-electronic transport. Ziese *et. al.* manipulated the interlayer coupling of $SrRuO_3/La_{0.7}Sr_{0.3}MnO_3$ superlattices and demonstrated a strong antiferromagnetic coupling depending upon the degree of Mn/Ru intermixing at the interface [64]. As a very thin $SrTiO_3$ layer was introduced between the $La_{0.7}Sr_{0.3}MnO_3$ and $SrRuO_3$ layers, a drastic suppression of the antiferromagnetic interlayer coupling was noticed, indicating the importance of the direct linking between the layers to maintain the coupling. We find that previous studies mainly focused either on the superlattices or on the mono-/bi-layers of SRO and LSMO, however, the role of the metallic paramagnet (such as LNO) and its interface on the overall charge transport and magnetic features of SRO/LSMO layers have been virtually unexplored so far. In the present work we propose such combination of materials design of various thickness levels on two different crystallographic orientations and report the global magneto-electronic transport of the trilayer system. Our main emphasis is on the temperature and magnetic field dependence charge transport in LSMO/LNO/SRO trilayer (TL) system grown on (001) and (111) single crystal $SrTiO_3$ substrates. Interestingly, the low-temperature magneto-transport studies reveal the interface driven Kondo like behavior which appears to be sensitive to the thickness of the ferromagnetic layers.

The structure of our paper is as follows. In Sec.II we present the experimental details which is followed by results pertaining to variation of resistivity with temperature and applied magnetic field and relevant discussion in Sec.III. Finally we conclude our observations in Sec.IV.

II. EXPERIMENTAL DETAILS

The dnm-SRO/3nm-LNO/dnm-LSMO trilayers [d=2.5(TL1), 5(TL2), 10(TL3), 15 (TL4)] comprising of ferromagnetic $SrRuO_3$ (SRO) as top-layer and $La_{0.7}Sr_{0.3}MnO_3$ (LSMO) as bottom layer with paramagnetic $LaNiO_3$ (LNO) sandwiched between them were grown on (001)-oriented (labeled as $TL1_{(001)}$, $TL2_{(001)}$, $TL3_{(001)}$, $TL4_{(001)}$), and (111)-oriented (labeled as $TL1_{(111)}$, $TL2_{(111)}$, $TL3_{(111)}$, $TL4_{(111)}$) single crystalline $SrTiO_3$ (STO) substrates by pulsed laser ablation mechanism using the Excimer (KrF) laser of wavelength 248 nm and energy density 2 J/cm^2. Following parameters are used during the deposition of the thin films: (i)

constant substrate temperature of 700°C, (*ii*) base pressure 10^{-6} mbar, and (*iii*) dynamic oxygen partial pressure of 0.2 mbar. *In-situ* annealing has been done after the deposition at 400 mbar of O_2 at 700°C for 45 min.

Phillips X'pert MRD X-ray diffractometer with Cu-$K\alpha$ as radiation source ($\lambda \sim 1.5405$ Å) has been used to study the formation and crystal structure of these TLs including the individual layers. The corresponding crystal structure information has been provided in the supplementary information (Figs. S1 and S2). Magneto-transport measurements were carried out using a home-made resistivity setup based on conventional four-probe method in the absence and presence of external magnetic field ($0 \leq \mu_0 H_{\rm DC} \leq 8$T). All the measurements were performed in the longitudinal geometry where the current was sent along the film-plane and the magnetic field was applied parallel to the current direction. The resistivity data as a function of temperature were recorded during warming for the temperature T = 5-300K. Temperature and field dependence of magnetic properties of the samples were investigated using superconducting quantum interference device (SQUID) magnetometer (Quantum Design). Ferromagnetic resonance (FMR) spectra were measured at room temperature using X-band (9.4GHz) Jeol Model(JES-FA200). As part of this measurement electron spin resonance were detected by applying the magnetic field that makes different angles (viz. $\theta = 0°, 45°, 90°$) with the plane of the TL.

III. RESULTS AND DISCUSSION

Figure 1 shows the temperature dependence of electrical resistivity $\rho(T)$ of the TLs films measured under zero magnetic field and in the presence of two different magnetic fields ($\mu_0 H_{\rm DC}$ = 0, 1 T and 8 T). Figures 1(*a-c*) represent the $\rho(T, \mu_0 H_{\rm DC})$ for $TL2_{(001)}$, $TL3_{(001)}$, and $TL4_{(001)}$ trilayer, respectively. Similarly, Figs. 1(*d-f*) show the $\rho(T, \mu_0 H_{\rm DC})$ of the $TL2_{(111)}$, $TL3_{(111)}$, and $TL4_{(111)}$. $TL1_{(001)}$ sample exhibits complete insulating behaviour throughout the temperature scale (see Fig. S3 of supplementary data), whereas, $TL2_{(001)}$ sample displays the metallic behaviour with metal-insulator transition (T_{MI}) around $T \sim 200$ K. On the other hand, all other samples show completely metallic behaviour for different (LSMO and SRO) thicknesses. Such higher order of magnitude in the electrical resistivity was reported in the literature with decreasing thickness of the film in monolayers and heterostructures of LSMO and SRO[65–67]. The metallic behaviour increases progressively with increasing the externally applied magnetic field. As the temperature is lowered (T<50K) resistivity values exhibit further drop upon increasing in $\mu_0 H_{\rm DC}$ ($\geq$ 1T). The minimum values of resistivity for metallic behaviour of TLs are observed when the temperature reaches around $T \sim 50$ K with an observable minimum resistivity up to $T \sim 15$ K. However, at low-temperature (for T < 15 K) a gradual rise in the resistivity was noticed for all the samples except for $TL1_{(001)}$ (see Fig. S3 of supplementary data). In the case of zero magnetic field, the maximum resistivity was obtained for all the samples below T = 10 K along with decrease in electrical resistivity upon increase in the applied magnetic field.

At low temperatures, the total electrical resistivity can be represented as the sum of inelastic and elastic scatterings, i.e. $\rho = \rho_{\rm elastic} + \rho_{\rm inelastic}$. Here, the elastic scattering process is mainly originated from the columbic interaction of charge carriers, while the inelastic scattering appears solely due to the interactions among the charge carriers, like, electron-phonon and electron-Magnon scattering processes[68,69]. In the present study in order to quantify the upturn observed at the low temperature in the electrical resisitvity (see Fig. 1), we have incorporated an additional term (ρ_{upturn}) in the electrical resistivity which results:

$$\rho = \rho_{elastic} + \rho_{inelastic} + \rho_{upturn} \quad (1)$$

At this stage to analyze the metallic behaviour appropriately we divide the regions in two parts:(*i*) temperature between 5 K and 50 K, and (*ii*) temperature between 50 K and 150 K. By considering the first part of the metallic region (5 K $\leq T \leq$ 50 K) for all samples, we have analysed the electrical resistivity data using the

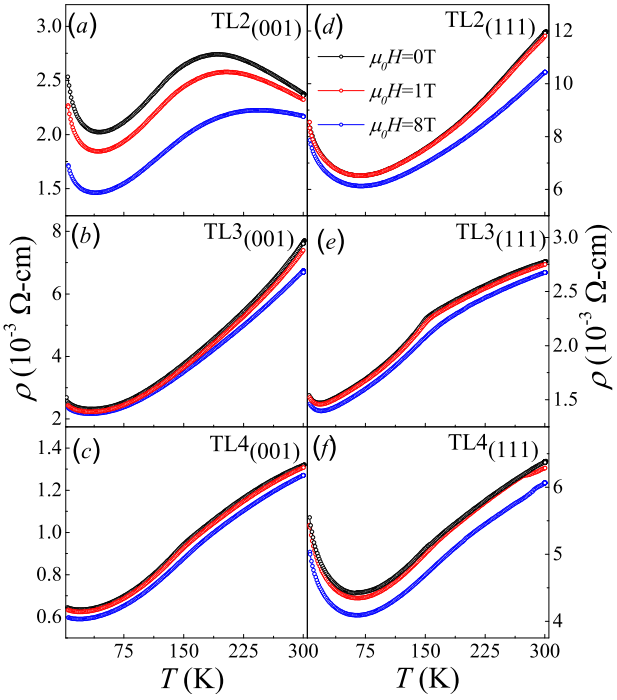

FIG. 1. Temperature variation of the electrical resistivity $\rho(T)$ of the trilayer films grown on (001)-oriented STO (*a-c*) and (111)-oriented STO (*d-f*) in the presence of different magnetic fields $\mu_0 H$ = 0 T, 1T and 8 T. At low temperature upturn in the ρ indicate the presence of Kondo like effect.

relation[56,70,71]

$$\rho = \rho_0 + \rho_5 T^5 + \rho_{1/2} T^{1/2} - \rho_1 lnT \quad (2)$$

where ρ_0 represents residual resistivity, second term (T^5) denotes the contributions due to inelastic scattering, third term ($T^{1/2}$) due to the electron-electron scattering and last term (lnT) represents spin dependent Kondo like effect. In Fig. 2, we have shown the scattered symbols as experimental data points, whereas, the solid line are best fits to the Eq.(2). The corresponding fitting parameters evaluated using the above relation are listed in the Table SI(supplementary). Overall we find decrease in the residual resistivity (ρ_0) with increase in the applied magnetic field. In order to understand the resistivity upturn in the TLs, we fitted the low temperature resistivity with both lnT and $T^{1/2}$ as shown in the insets of Fig. 2. Apparently, fitting with the lnT term appears to be more closer to the current experimental results than the fitting corresponding to $T^{1/2}$ term. This senario suggests the presence of low temperature Kondo effect in these TLs and the importance of interface effects. It is now quite evident from the Table SI (supplementary data) that for $TL_{(001)}$ the constants ρ_1 and $\rho_{1/2}$ exhibit decreasing trend with the increase of the layer thickness. In case of $TL_{(111)}$ we are unable to notice any systematic trend. At low temperature range the observed fitting parameters suggest a competition between the Kondo term and the electron-electron interaction. Interestingly the electron-electron interaction exhibits increasing trend on the expense of decreasing trend in the Kondo effect.The magnitudes of the constant ρ_1 is one order larger than $\rho_{1/2}$, which also reveals the dominance of the Kondo effect in the TLs.

Usually, in the case of conventional Kondo effect, the logarithmic temperature dependence of electrical resistivity is related to the spin dependent transport behavior of electrons (interaction between the conduction electrons and the localized spin impurities). Even though the upturn in the resistivity is noticed earlier in thinner (< 10nm) SRO layers[42], our current observations present a strong evidence of low-temperature increase in the resistivity for moderately thicker SRO and LSMO layers with very thin LNO as a spacer. However, our results (see the supplementary information Fig. S4) pertaining to the single layers (of SRO, LNO and LSMO) did not show any signature of upturn. In this case, the top layer SRO plays a central role along with the interface of the TLs. Generally, the interaction of the localized impurities with the conduction electrons at the interface may be attributed to the origin of Kondo like behavior in these systems[72]. The oxygen vacancies across the disordered interfaces (altered bond geometry) may influence the generation of localized spins that can interact with the unpaired electrons mainly coming from the ruthenium in SRO and from nickel in LNO[30]. Also, the altered interfacial charge transfers between the cations (Ru^{4+}-O^{2-}-Ni^{2+} and Ru^{4+}-O^{2-}-Ni^{3+}) may play a significant role in the overall transport properties. The reduction of the resistivity in presence of high magnetic field (i.e. 8 T) can be attributed to the suppression of spin dependent scattering. However in our system, we would like to point that the LSMO exhibits strong ferromagnetic behaviour with high value of magnetic moment ($3.7\mu_B$) which is the reason of the suppression of the localized magnetic moment even at high external field. This reveals that the SRO/LNO interface may be held responsible for the increase in the resistivity upturn at low temperatures in our present TL systems.

In the case of the Kondo effect, the minimum values of electrical resistivity may arise due to the electron scattering with magnetic impurities situated at non-magnetic lattice. It is also possible that Kondo effect can appear in the ferromagnetic materials[73,74]. Kondo effect could be screened by the spin exchange coupling (J) and the existence of spin singlet state between the conducting electrons and localized magnetic moment of the impurities below a characteristic temperature $T_K \approx D/k_B[\exp(-1/Jd(E_F)]$[75,76]. Here, D represents the conduction bandwidth, $d(E_F)$ the density of states at Fermi energy level and k_B the Boltzmann constant.

As temperature continuously decreases, the extent of electrons confinement at the Fermi surface increases that leads in the spin scattering as a result of this scattering amplitude tends to infinity. Therefore, in order to understand the contribution of spin dependent magnetic impurities in the resistivity upturn at low temperature, we analyze the data by considering an empirical formula, $\rho_m(T) = \rho_0[1 + (2^{1/\alpha_s} - 1)(T/T_K)^{\xi_s}]^{-\alpha_s}$ obtained from the numerical renormalisation group (NRG) method[77]. In the above expression, exponents ξ_s and α_s are the fitting parameters and ρ_0 is residual resistivity. For the TLs our fitting analysis yields the following parameters $\xi_s \sim 0.95(1.81)$, $\alpha_s \sim 0.05(0.06)$ and Kondo temperature $T_K \sim 0.13$ K (0.31 K) for $TL2_{(001)}$ ($TL2_{(111)}$), respectively. The NRG fitting analysis is given in the Fig. S5 (supplementary data) and the corresponding fitting paramters are listed in Table SII (supplementary data). Similar type of results is reported in the case of 4.5% Pt doped $Mn_{50.5}Bi_{45}$ alloys and AgFe with $\xi_s \sim 2$ and $T_K \sim 5$ K corresponding to the spin S = 3/2.[77]

For $T > T_K$ the resistivity data fit well with the relation

$$\rho(T) = \frac{\rho_0 \pi^2 S(S+1)}{4(ln(T/T_K))^2}\left[1 - \frac{3\pi^2 S(S+1)}{4(ln(T/T_K))^2}\right] \quad (3)$$

and results S = 1/2 (3/2) with $T_K \sim 9.19\times10^{-7}$ K (3.09×10^{-4} K) for the trilayers $TL2_{(001)}$ ($TL2_{(111)}$). In Fig 3 we show the fitting of the experimental data with the above mentioned relation (Eq.(3)) with the solid lines. These fitting parameters suggest that magnetic impurities responsible for the Kondo scattering are not entirely screened at the lowest measuring temperature in the LSMO/LNO/SRO TLs. The temperature (T_M) at which minimum in the resistivity (ρ_M) occurs gradually shifts towards lower temperatures with increasing the strength of the magnetic field. For the samples $TL2_{(001)}$, ρ_M occurs at T_M = 43.77 K, 43.45 K, and 37.94 K

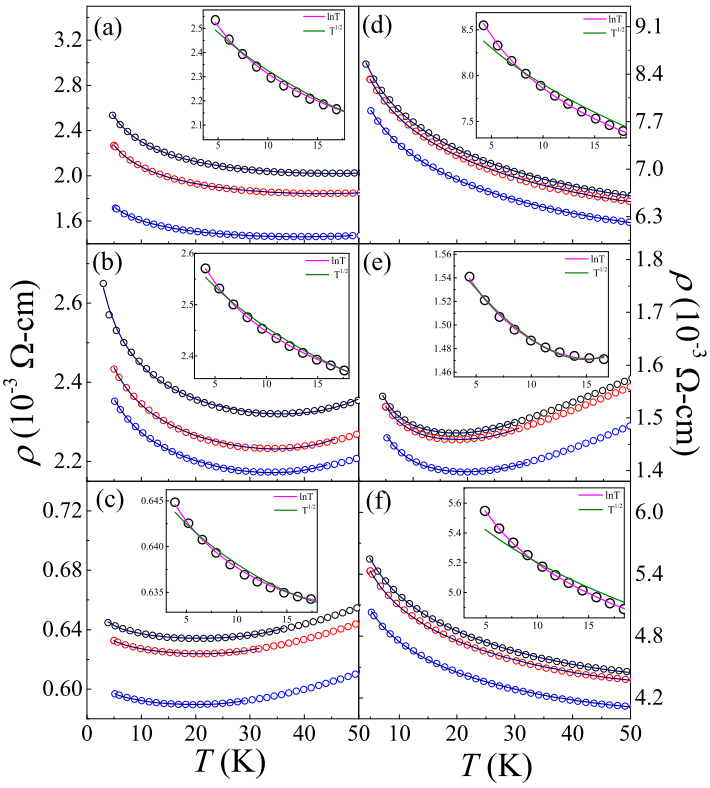

FIG. 2. Low temperature resistivity $\rho(T)$ curves fitted with the relation (Eq.2) for the trilayers grown on (001)-oriented STO (a) $TL2_{(001)}$, (b) $TL3_{(001)}$, and (c) $TL4_{(001)}$ and (111)-oriented STO (d) $TL2_{(111)}$, (e) $TL3_{(111)}$, and (f) $TL4_{(111)}$. The black, red and blue scattered symbols represent experimental data points measured at different fields $\mu_0 H = 0$, 1 and 8T, respectively. The solid lines represent best fits to the Eq.(2).

for $\mu_0 H_{\rm DC}$ = 0 T, 1 T and 8 T, respectively. For the TLs $TL3_{(001)}$ ($TL3_{(111)}$), and $TL4_{(001)}$ ($TL4_{(111)}$) we obtained $T_K \sim 1.07\times10^{-5}$ (1.06×10^{-9}) and 1.38×10^{-17} (1.52×10^{-7}), respectively. In addition, the TLs $TL3_{(001)}$ and $TL4_{(111)}$ exhibit $S = 3/2$, however, the TLs $TL3_{(111)}$ and $TL4_{(001)}$ show remarkably high magnitude of S. The resistivity data for other four TLs fit quite well with Hamann's relation (Eq.3). The corresponding analysis is provided in the supplementary material (Fig. S6).

Other possible reason for getting upturn in the resistivity at low temperatures maybe attributed due to the quantum interference effect (QIE)[55]. Such effect induces a positive magneto-resistance in manganite materials due to the inevitable contribution of spin-orbit coupling in weak localization which finally leads to anti-localization. Nevertheless, in our present systems, we noticed negative magneto-resistance (see Fig. 4) which indicate the contribution of weak localization in the system. Therefore we conclude that, in our TLs, the interface has different spin structure than the core ferromagnet which drives the system to Kondo like effect in the resistivity data. In addition, there are other dominant factors like grain boundaries and phase separation that may destroy the Kondo effect in the presence of external applied magnetic field.

In the temperature regime ($T>$ 50 K), the electrical resistivity data can be associated with the relation:

$$\rho = \rho_0^{'} + \rho_2^{'} T^2 + \rho_5^{'} T^5 \qquad (4)$$

where $\rho_0^{'}$ represents residual resistivity, second term attributes to the delocalized electron-electron scattering (EES) and last term corresponds to the electron-phonon scattering (EPS) mechanism. The term $T^{1/2}$ in the Eq. 2 is due to the localized electron-electron correlations at low temperature, however, the term T^2 comes due to the delocalized electron-electron correlation. The origin of the former is solely quantum mechanical in nature, while later is classical[78]. In general, the charge transport of a traditionally weak disorder system can be represented as $\rho(T) \propto T^n$, where $n = 2$ is a conventional electron electron scattering described by classical Fermi liquid (FL) model[79]. However, at low temperature, the classical FL model fails to explain the unusual behavior (such as upturns appears due to the Kondo effect) and the quantum corrections are needed to explain the features. Such corrections are required to take account of inelastic scattering and the presence of random fluctuations in time evaluation of the electronic states[80]. Therefore, the quantum interference or localization effects at

low temperatures can be attributed to the greater inelastic scattering time (τ_{in}) compared to the elastic scattering time (τ). The temperature dependent of conductivity with different power law exponent has been considered for layers whose thickness is less than the coherence length ($L_{coh} = (D\tau_{in})^{1/2}$, with D as a diffusion constant) consequently the electron - electron interaction follows the relation $\sigma(T) = \sigma_0 + AT^{1/2}$ for 3D system[78,80].

The solid lines in Fig. S7 (supplementary data) represent the best fits of Eq.(4) with the experimental $\rho(T)$ data for all the samples measured at three different fields ($\mu_0 H$ = 0, 1, 8 T). Here, we find that the experimental data fit quite well with the mixed state configuration (EES and EPS) of $\rho(T)$. In the conventional metals it is very difficult to observe the domination in the resistivity that occurs due to electron-phonon scattering or by the impurity scattering. Here, the combined effect of both EES and EPS appears to be more appropriate to explain the nature of experimental data of electrical resistivity for the LSMO thin films[81]. These two mechanisms are usually opposite to each other depending upon the measuring temperature and disorder at the interface. In the present case EPS exhibits decreasing trend with decrease in temperature, but the electron-electron scattering increases progressively with the reduction of temperature. As we carefully analyze the data we find that the contribution from the electron-electron scattering dominates compared to the electron-phonon scattering in the temperature range between 50K-150K which is quite evident from the obtained fitting resistivity coefficients ρ_2' and ρ_5'. The parameters are presented in the Table SIII (supplementary data). As we look at the variation of residual resistivity coefficients with the applied field we find that it does not show any significant change for a given thickness. We could not able to figure out any significant variation in the residual resistivity by varying the thickness for a given magnetic field. In general, the electron-phonon scattering (EPS) dominates on the electron-electron scattering (EES) at high temperature due to the presence of the three order high exponent in former contribution compared to the later. However, in the TL systems, we find that the EES coefficients are nearly 10^6 time larger than the EPS coefficients for entire range of temperature and all the magnetic fields.

In our case none of the isolated terms in the above Eq.(4) are perfectly fitting with the experimental data. From the Eqs.(2) and (4), we find that the minimum value of resistivity have the mixed contribution from both electron-phonon and electron-electron scattering mechanisms. Previous studies by Bhattacharya *et. al.* observed eight orders of increase in the magnitude of in-plane resistivity values of $(LaMnO_3)_{2n}/(SrMnO_3)_n$ superlattices with increasing the n values from 1 to 5 unit cells. However, an insulating behaviour was observed for

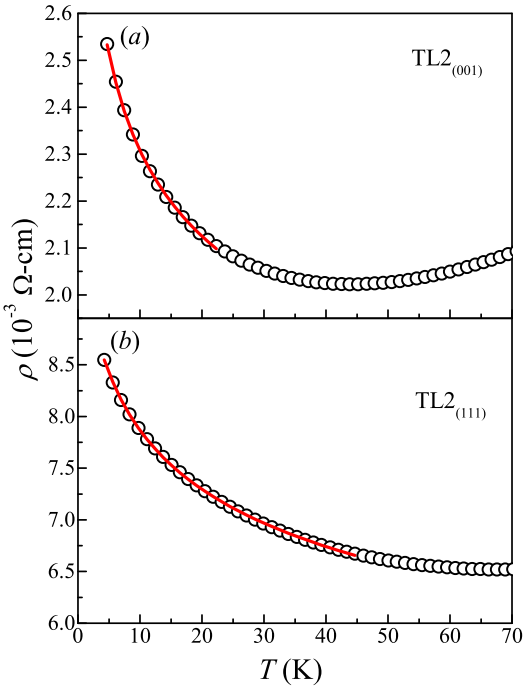

FIG. 3. Temperature dependence of electrical resistivity $\rho(T)$ curves at $T > T_K$ of the trilayers (*a*) $TL2_{(001)}$, and (*b*) $TL2_{(111)}$ after fitting with the Eq.(3) given in the text. Here the black open circles represent experimental data points, and the red color solid lines represent best fits to the Eq.(3).

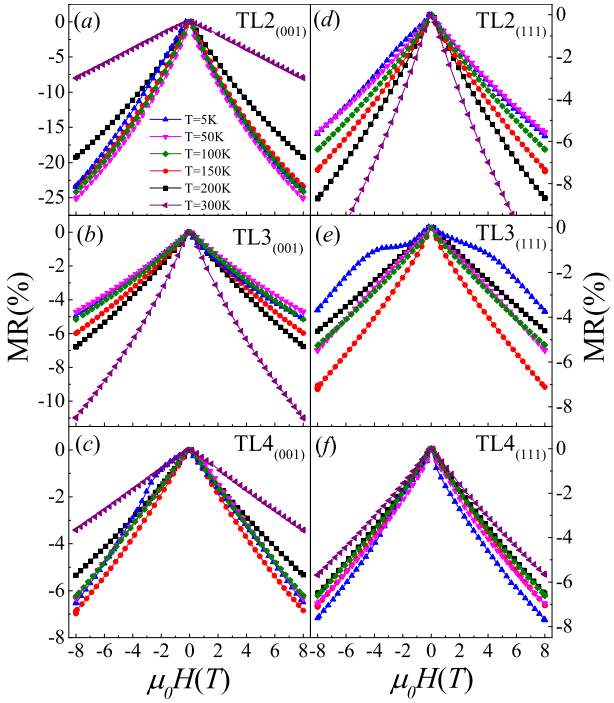

FIG. 4. Magneto-resistance (MR) $[\Delta\rho/\rho = (\rho(H) - \rho(0))/\rho(0) \times 100)]$ versus field measured at selected temperatures (T = 5, 50, 100, 150, 200 K and 300 K) for the trilayers of different thickness grown on (001)-oriented STO (*a-c*) and (111)-oriented STO (*d-f*).

$n \geq 3$ [82]. In case of $[(La_{0.7}Sr_{0.3}MnO_3)_5$-$(LaNiO_3)_n]_{12}$, $[(LaNiO_3)_n/(LaMnO_3)_2]$, and $[(LaNiO_3)_n/(SrMnO_3)_2]$ superlattices an insulating to metallic crossover was observed with increasing the thickness of LNO more than three unit cells which is accompanied by the interface charge transport due to Ni^{2+} to Ni^{3+} [38,83–85].

Fig. 4 depicts the magnetic field variation of magneto-resistance given as $MR(\%) = (\rho(H) - \rho(0))/\rho(0) \times 100$, measured at different temperatures (5 K $\leq T \leq$ 300 K) for the TLs. The current high temperature MR curves exhibit linear variation with magnetic field due to the electron-phonon contribution. However, a slight deviation from the linear behaviour was observed at low temperature MR due to the spin contribution[86]. This effect is more pronounced particularly in Fig. 4(e). Nevertheless, all samples exhibit negative magneto-resistance in the entire temperature range without any systematic trend possibly either due to the combined influence of quantum-interference-effects (QIE) accompanied by the spin-orbit coupling or due to the weak localization-effects (WLE). In the former case the impurity induced electron-electron correlations play a significant role on the global MR behaviour. Usually, if both QIE and WLE are present in the system one should observe positive magneto-resistance at lower fields due to the dominant role of spin-orbit coupling which is generally noticed in SRO thin films[48]. However, in the present case we did not observe such positive MR in SRO/LNO/LSMO TLs either on (001)-STO or (111)-STO. Thus ruling out the contribution of spin-orbit interaction that supports the Kondo like features at low temperature ($T \leq$ 10K). Usually, low-field polarity switching in MR represents strong anisotropic magneto-resistance whose magnitude and sign depend on the direction of externally applied magnetic field[44,88].

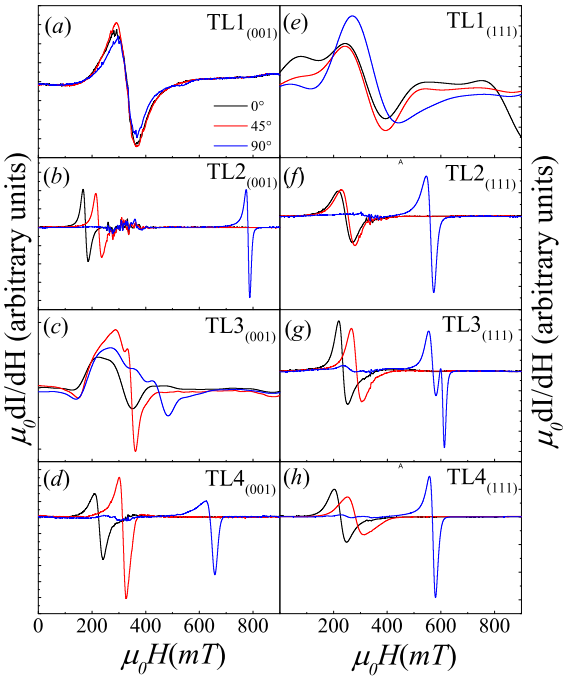

FIG. 5. Room temperature ferromagnetic-resonance (FMR) spectra of the trilayer of different thickness grown on (001)-oriented STO (a-d) and (111)-oriented STO (e-h).

We deduced the information related to the magnetic structures of these TLs using the differential resistivity ($d\rho/dT$) and compared with the direct temperature dependence of the magnetization (M(T)) measurements. In Fig. S8 (Supplementary data) we show the first derivative of resistivity ($d\rho/dT$) as a function of temperature of the TLs ($TL2_{(001)}$, $TL2_{(111)}$, $TL4_{(001)}$, and $TL4_{(111)}$). Interestingly, we find that in the case of $TL2_{(001)}$ two peaks are observed around $T_{p1} \sim$ 104K and $T_{p2} \sim$123 K, whereas, the rest of the TLs show only one broadened peak. The peak T_{p2} is associated with the ferromagnetic phase transition ($T_{C\text{-}SRO}$) of SRO, whereas, the peak T_{p1} is related to either the superparamagnetic blocking or spin-glass freezing temperature, which are related to the finite size effects of the TLs[30]. As the external magnetic field is increased the peak broadening associated to the $T_{C\text{-}SRO}$ slightly shifts to high temperature regime which is typical to any ferri/ferromagnetic system. Such field-induced broadening of the magnetic transition is more prominent at high fields for the TLs on (111)-STO as compared to TLs on (001)-STO, inferring the dominant field-induced-anisotropy (dT_{p2}/dH) in these systems. Upon varying the thickness ($TL_{(001)}$) of both the ferromagnetic constituents SRO and LSMO of the TLs the peak corresponding to T_C gradually shifts towards higher temperature side (140K). Similar high temperature shifting has been noticed for $TL2_{(111)}$ (∼146K) as well as $TL4_{(111)}$ (∼150K). These results are consistent with the temperature dependence of differential magnetization curves $\partial M(T)/\partial T$ obtained from the M(T) curves recorded under both zero-field-cooled (ZFC) and field-cooled (FC) conditions for different magnetic field ($\mu_0 H$ = 0T, 1T and 8T). Previous studies by Schultz *et. al.* reported similar observations in ultrathin SRO single layers for different thicknesses in which the peak corresponding to $d\rho/dT$, across the ferromagnetic transition of SRO gradually increases with increasing the SRO layer thickness[87].

Next we turn our focus to analyze the response of the material on the externally applied magnetic field. To probe anisotropy effects we performed field dependent ferromagnetic-resonance (FMR) of the TLs at room temperature for different measuring angles ($\theta = 0°$, 45° and 90°) between the magnetic field and the plane of the TL. Fig. 5 shows the FMR spectra recorded at room temperature at a constant frequency (f) of 9.4 GHz for all the TLs. The resonance magnetic field ($\mu_0 H_R$) and peak to peak linewidth ($\mu_0 \Delta H_{PP}$) are estimated from the absorption spectra fitted to the Lorentz line shape. As the angle (θ) between the magnetic field and plane of the film increases $\mu_0 H_R$ gradually shifted towards the higher fields consistent with large anisotropy of the trilayers. However, this shifting towards higher fields is not visible

TABLE I. Different magnetic parameters evaluated using Eqs.(5) and (6) for our experimental data of different trilayers. From left to right table represents sample, saturation magnetization (M_S), In-plane resonance magnetic field ($\mu_0 H_\parallel$), In-plane peak to peak resonance ($\mu_0 \Delta H_\parallel$), Out-of-plane resonance magnetic field ($\mu_0 H_\perp$), Out-of-plane peak to peak resonance ($\mu_0 \Delta H_\perp$), Effective magnetic anisotropy (K_{eff}), respectively.

Sample	M_S (emu/cc)	$\mu_0 H_\parallel$ (mT)	$\mu_0 \Delta H_\parallel$ (mT)	$\mu_0 H_\perp$ (mT)	$\mu_0 \Delta H_\perp$ (mT)	K_{eff} (10^5 J/m^3)
$TL1_{(001)}$	72	324.75	125	324.31	114.31	0.25
$TL2_{(001)}$	106	176.57	90.33	778.25	21.57	2.07
$TL3_{(001)}$	240	357.53	79.54	314.47	109.45	2.87
$TL4_{(001)}$	280	219.92	64.11	630.75	57.62	3.62
$TL1_{(111)}$	124	328.57	90.91	375.27	318.19	0.75
$TL2_{(111)}$	180	243.98	81.08	555.89	45.49	1.77
$TL3_{(111)}$	227	239.56	65.91	572.55	33.98	2.45
$TL4_{(111)}$	260	227.26	77.11	565.07	44.74	3.17

in the case of $TL1_{(001)}$. Particularly, the high magnitude of out-of-plane $\mu_0 H_R$ is arising due to the major contribution of magneto-crystalline anisotropy. Hence to quantify the magnetic anisotropy and to verify the contribution of the anisotropy of TLs, we have analyzed the FMR spectra in terms of Kittels dispersion relation given below[89,90]:

$$\left[\frac{\omega}{\gamma}\right]^2 = H_\parallel[H_\parallel + 4\pi M_s - H_a] \quad (5)$$

$$\frac{\omega}{\gamma} = [H_\perp - (4\pi M_s - H_{a1})] \quad (6)$$

In the above equation (Eqs. 5 and 6), ω is the angular frequency, γ corresponds to the gyromagnetic ratio of the electron, $4\pi M_s$ attributes the shape anisotropy, the anisotropy field H_a(=H_{a1}+H_{a2}) and H_{a1} and H_{a2} represent the magnetic anisotropic fields of the film along the film plane and out-of-plane, respectively. Both the parameters H_{a1} and H_{a2} are related to the anisotropy constants K_1 and K_2 with the relations $H_{a1} \sim \mid 2K_1/M_s \mid$ and $H_{a2} \sim \mid 4K_2/M_s \mid$. All the estimated parameters are listed in Table I. Here, the in-plane magnetic anisotropy value originated due to the global effect of shape, exchange, and magneto-crystalline anisotropies of the TLs. Thus, we have evaluated the effective magnetic anisotropy ($K_{eff} = K_\nu + K_s/t_{FM}$), from the average values of K_1 and K_2, where, K_{eff} value depends on the thickness of the ferromagnetic layer (t_{FM}), and surface and volume anisotropies (K_ν and K_s). In Fig. 6 we plot the effective anisotropy versus LSMO thickness of the TLs, which exhibits linear variation. The estimated value of anisotropies are K_ν =4.04×10^5 J/m^3 (3.31×10^5 J/m^3), and K_s = -9.57×10^{-4} J/m^2 (-6.68×10^{-4} J/m^2) for the TLs on (001)-STO (TLs on (111)-STO). The positive sign of K_ν indicates the volume anisotropy perpendicular to film anisotropy and the signs of K_s are opposite. Positive sign corresponds the easy uniaxial axis parallel to the normal of the film for TL and the opposite one indicate the easy axis associated with the plane of the film[91].

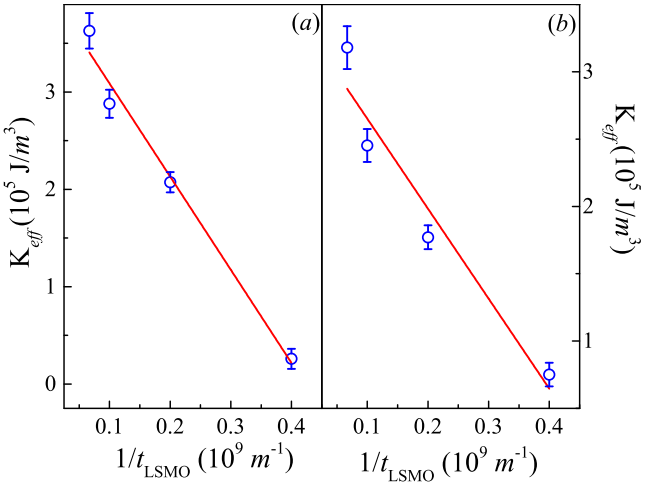

FIG. 6. The effective anisotropy (K_{eff}) versus reciprocal of LSMO thickness ($1/t_{LSMO}$) for the trilayers on (*a*) 001- and (*b*) 111-oriented STO substrate. The solid red line represents the linear fit.

For all the TL samples the in-plane and out-of-plane FMR linewidths significantly alter with the ferromagnetic layer thickness. Usually, the $\mu_0 \Delta H_{PP}$ values quantify the anisotropic field based on the narrowness of the FMR signal. Whereas, the broadening signifies phenomenological Gilbert damping (how fast the magnetization switches along the applied field direction) and 2-Magnon scattering[92,93]. On the other hand, the magnitude of $\mu_0 \Delta H_{PP}$ is very useful for the investigation of the underlying intrinsic dynamical mechanisms, extrinsic structural inhomogeneities, and defects in the system. In general, more dominant part of the linewidth is

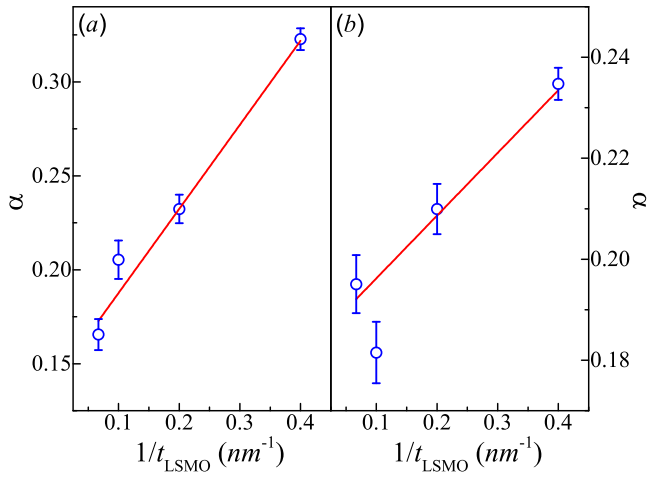

FIG. 7. LSMO thickness variation of Gilbert damping coefficient $\alpha(1/t_{\rm LSMO})$ for different thickness of trilayers on (a) 001- and (b) 111- oriented STO substrate. The solid red line represents the linear fit.

contributed from the in-plane than the out-of-plane linewidth, $\Delta H_{\parallel}>\Delta H_{\perp}$. Furthermore, the in-plane linewidth ($\Delta H_{\parallel}$) values strongly influenced by the orientation of magnetization and the nonlinearity in their values. This effect generally arises due to the 2-Magnon scattering. Therefore, for sake of simplifying the analysis, here, we assume that the intrinsic behaviour of the TL could be contributed from the in-plane linewidth of the FMR signal. In general, the FMR linewidth and Gilbert damping coefficient (α) are related as $\alpha = (\sqrt{3}\gamma\Delta H)/2\omega$[94,95]. The Gilbert damping constant varies between 0.32(0.23) and 0.16(0.19) for the TL on (001)(TL on (111)). The estimated values of α are higher than the previous reported values 0.005 and 0.16 for monolayers LSMO and LSMO/Pt, respectively[96].

Fig. 7 depicts the LSMO thickness dependence of Gilbert coefficient $\alpha(t_{\rm FM})$ that shows an increasing trend with decrease in the film thickness signifying the delay in magnetization switching in TLs. The total magnetic relaxation of the TL is deduced from the relation $\alpha = \alpha_0+\gamma/(4\pi M_s)(\hbar g^{\uparrow\downarrow}/t_{\rm FM})$[97]. Here, M_s is the saturation magnetization, γ represents the gyromagnetic ratio, α_0 is the residual Gilbert constant and $g^{\uparrow\downarrow}$ represents spin mixing conductance. For the current TL system on (001) and (111) the magnitude of spin conductance is estimated as 5.19×10^{19} and 13.38×10^{19} m^{-2}, respectively, which are comparable to the previously reported values for Pt/LSMO bilayer films[97].

IV. CONCLUSIONS

In this paper we have presented a systematic study on the thickness and magnetic field dependence of electronic transport, and ferromagnetic resonance of ultrathin SRO/LNO/LSMO TLs on (001)- and (111)-STO. We have demonstrated that these TLs undergo a metallic to insulating state upon decreasing the thickness of both the ferromagnetic constituents. The TLs show unusual charge transport at low temperature similar to the Kondo like behaviour with interesting interplay of the disorder across interfaces and the size-effects.

Below a critical temperature $T_{\rm M}$, the electrical resistivity (ρ) exhibits logarithmic (lnT) as well as power law ($T^{1/2}$) dependence on the temperature revealing an existence of mixed state behaviour of both Kondo like spin dependent effects and electron-electron scattering. In order to probe the Kondo screening, we analyzed the upturn in $\rho(T<T_{\rm M})$ with the help of numerical renormalization group method for $T<T_{\rm K}$ ($T_{\rm K}$ being the Kondo Temperature) and Hamann's resistivity relation $\rho(T) \propto (ln(T/T_{\rm K}))^{-2}$ in the region where $T>T_{\rm K}$. Using the Hamann's approach the contribution of spin and $T_{\rm K}$ are deduced as S = 1/2 (3/2) and $T_{\rm K} \sim 9.19\times10^{-7}$ K (3.09×10^{-4} K) for the TLs $TL2_{(001)}$ ($TL2_{(111)}$). Apart from these important features, negative magneto-resistance (MR) complements the presence of Kondo like behavior in these TLs, which increases with the reduction of the thickness divulging the 2D weak localization effect originating due to the electron-phonon collisions. At the temperatures $T \gg T_{\rm K}$, electron-electron ($\rho(T) \propto T^2$) and electron-phonon ($\rho(T) \propto T^5$) interactions dominate with negligible contribution from the 2-Magnon scattering. These peculiar results infer that the low temperature Kondo like effect appears owing to the interaction between the localized impurities and the conduction electrons at the interface of SRO and LNO. Although the resistivity upturn is a well-established feature in thinner (< 10nm) SRO layers, the present trilayer system exhibits the similar trend for comparatively thick SRO and LSMO layers with very thin LNO as a spacer. Thus the interface between the layers play a dominant role on the overall charge transport in the TLs mainly driven by the altered interfacial charge transfers between the cations.

From the in-plane and out-of-plane ferromagnetic resonance (FMR) spectra, the estimated volume and surface magnetic anisotropies are, $K_\nu \sim 4.04\times10^5$ J/m^3 (3.31×10^5 J/m^3) and $K_s \sim$ -9.57$\times10^{-4}$ J/m^2 (-6.68 $\times10^{-4}$ J/m^2) for the $TL_{(001)}$ ($TL_{(111)}$). These anisotropy values are in good agreement with the earlier reports[97]. These TLs exhibit one order higher in magnitude of Gilbert damping constant as compared to the single layer LSMO and LSMO/Pt, which indicates the slowdown in the magnetization while transferring the spin to LSMO through LNO layer. Using the FMR data we have evaluated the spin mixing conductance $g^{\uparrow\downarrow} = 5.2\times10^{19}m^{-2}$ and $13.38\times10^{19}m^{-2}$ for the TL on (001) and TL on (111) oriented STO, respectively. Finally, we established a systematic correlation between the differential resistivity and the magnetic ordering temperatures and deduced the magnetic structure in which the field-induced anisotropic broadening (dT_c/dH) has been noticed.

V. ACKNOWLEDGMENTS

SG, RGT, PP, DCJ, PKM and ST acknowledge the support from UGC-DAE CSR, Indore for providing the temperature-dependent electrical and magnetic transport measurement using the conventional four probe method and the temperature dependent magnetic measurements using SQUID. In particular we express our gratitude and sincere thank to Dr. R. Rawat and Sachin Kumar for helping us in electrical measurement, and Dr. R. J. Choudhary for the support in the magnetic measurement. SG, RGT, PP, DCJ also thanks the Central Instruments Facility (CIF)-IIT Guwahati for the partial support of this work.

[1] H. Y. Hwang, Y. Iwasa, M. Kawasaki, B. Keimer, N. Nagaosa, and Y. Tokura, Nat. Mater. **11**, 103 (2012).
[2] C.-H. Chang, A. Huang, S. Das, H.-T. Jeng, S. Kumar, and R. Ganesh, Phys. Rev. B **96**, 184408 (2017).
[3] P. Zubko, S. Gariglio, M. Gabay, P. Ghosez, and J.-M. Triscone, Annu. Rev. Condens. Matter. Phys. **2**, 141 (2011).
[4] Sujit Das, Andreas Herklotz, Er Jia Guo, and Kathrin Dörr, J. Appl. Phys. **115**, 143902 (2014)
[5] S. Thota, K. Roychowdhury, V. Thakare, S. C. Ganguli, Z. H. Chen, E. J. Guo, and S. Das, Appl. Phys. Lett. **113**, 122405 (2018)
[6] Y. Wang, R. Ramaswamy, and H. Yang, J. Phys. D Appl. Phys. **51**, 273002 (2018).
[7] L. Samet, D. Imhoff, J.-L. Maurice, J.-P. Contour, A. Gloter, T. Manoubi, A. Fert, and C. Colliex, Eur. Phys. J. B **34**, 179 (2003).
[8] M. Bibes, J. E. Villegas, and A. Barthelemy, Adv. Phys. **60**, 5 (2011).
[9] B. Dieny, V. S. Speriosu, S. S. Parkin, B. A. Gurney, D. R. Wilhoit, and D. Mauri, Phys. Rev. B **43**, 1297 (1991).
[10] M. Bibes and A. Barthelemy, IEEE Trans. Electron Devices **54**, 1003 (2007).
[11] J. Ma, X. Liu, T. Lin, G. Gao, J. Zhang, W. Wu, X. Li, and J. Shi, Phys. Rev. B **79**, 174424 (2009).
[12] P. Yu, J.-S. Lee, S. Okamoto, M. Rossell, M. Huijben, C.-H. Yang, Q. He, J. Zhang, S. Yang, M. Lee, et al., Phys. Rev. Lett. **105**, 027201 (2010).
[13] G. S. Bhalla, P. B. Rossen, G. K. Pálsson, M. Mecklenburg, T. Orvis, S. Das, Y. L. Tang, J. S. Suresha, D. Yi, A. Dasgupta, D. Doenning, V. G. Ruiz, A. K. Yadav, M. Trassin, J. T. Heron, C. S. Fadley, R. Pentcheva, J. Ravichandran, and R. Ramesh, Phys. Rev. Mater. **2**, 102001(R) (2018).
[14] Sujit Das, Anirban Ghosh, Margaret R. McCarter, Shang-Lin Hsu, Yun-Long Tang, Anoop R. Damodaran, R. Ramesh and Lane W. Martin, APL Materials **6**, 100901 (2018).
[15] S. Dussan, A. Kumar, J. Scott, and R. S. Katiyar, Appl. Phys. Lett. **96**, 072904 (2010).
[16] S. Majumdar and S. van Dijken, J. Phys. D Appl. Phys. **47**, 034010 (2013).
[17] A. Haghiri-Gosnet and J. Renard, J. Phys. D Appl. Phys. **36**, R127 (2003).
[18] N. Izyumskaya, Y. Alivov, and H. Morkoc, Crit. Rev. Solid State Mater. Sci. **34**, 89 (2009).
[19] P. Kumar, P. Pal, A. Shukla, J. Pulikkotil, and A. Dogra, Phys. Rev. B **91**, 115127 (2015).
[20] E. Kirichenko, V. Stephanovich, and V. Dugaev, Phys. Rev. B **95**, 085305 (2017).
[21] V. Stephanovich and V. Dugaev, Phys. Rev. B **93**, 045302 (2016).
[22] V. Aswin, P. Kumar, P. Pal, and A. Dogra, Opt. Lett. **41**, 1134 (2016).
[23] C.-J. Li, H.-X. Xue, G.-L. Qu, S.-C. Shen, Y.-P. Hong, X.-X. Wang, M.-r. Liu, W.-m. Jiang, P. Badica, L. He, et al., Sci. Rep. **8**, 195 (2018).
[24] S. Das, A. Herklotz, E. Pippel, E. J. Guo, D. Rata, and K. Dörr, Phys. Rev. B **91**, 134405 (2015).
[25] X. Ke, L. Belenky, C. Eom, and M. Rzchowski, J. Appl. Phys. **97**, 10K115 (2005).
[26] S. Catalano, M. Gibert, J. Fowlie, J. iguez, J.-M. Triscone, and J. Kreisel, Rep. Prog. Phys. **81**, 046501 (2018).
[27] J. Torrance, P. Lacorre, A. Nazzal, E. Ansaldo, and C. Niedermayer, Phys. Rev. B **45**, 8209 (1992).
[28] M. L. Medarde, J. Phys. Condens. Matter. 9, 1679 (1997).
[29] S. Wu, S. A. Cybart, D. Yi, J. M. Parker, R. Ramesh, and R. Dynes, Phy. Rev. Lett. **110**, 067202 (2013).
[30] S. Thota, S. Ghosh, S. Nayak, D. Joshi, P. Pramanik, K. Roychowdhury, and S. Das, J. Appl. Phys. **122**, 124304 (2017).
[31] D. Zheng, C. Jin, P. Li, L. Wang, L. Feng, W. Mi, and H. Bai, Sci. Rep. **6**, 24568 (2016).
[32] G. Zhou, H. Ji, J. Zhang, Y. Bai, Z. Quan, and X. Xu, J. Mater. Chem. C **6**, 582 (2018).
[33] R. Rana, P. Pandey, R. Singh, and D. Rana, Sci. Rep. **4**, 4138 (2014).
[34] X. Ning, Z. Wang, and Z. Zhang, Sci. Rep. **5**, 8460 (2015).
[35] G. Zhou, F. Jiang, J. Zang, Z. Quan, and X. Xu, ACS Appl. Mater. & interfaces **10**, 1463 (2018).
[36] S. Das, A. D. Rata, I. V. Maznichenko, S. Agrestini, E. Pippel, N. Gauquelin, J. Verbeeck, K. Chen, S. M. Valvidares, H. Babu Vasili, J. Herrero-Martin, E. Pellegrin, K. Nenkov, A. Herklotz, A. Ernst, I. Mertig, Z. Hu, and K. Dörr, Phys. Rev. B **99**, 024416 (2019).
[37] S. Das, S. Ghosh, P. Pramanik, D. C. Joshi, and S. Thota, J. Phys. D: Appl. Phys. **51**, 325001 (2018).
[38] J. Hoffman, I. Tung, B. Nelson-Cheeseman, M. Liu, J. Freeland, and A. Bhattacharya, Phys. Rev. B **88**, 144411 (2013).
[39] J. R. Sánchez, B. Nelson-Cheeseman, M. Granada, E. Arenholz, and L. Steren, Phys. Rev. B **85**, 094427 (2012).
[40] M. Gibert, M. Viret, P. Zubko, N. Jaouen, J.-M. Tonnerre, A. Torres-Pardo, S. Catalano, A. Gloter, O. Stphan, and J.-M. Triscone, Nat. Commun. **7**, 11227 (2016).
[41] H.-J. Kim, D. G. Yoo, and S.-I. Yoo, Mater. Lett. **123**, 23 (2014).
[42] X. Ning, Z. Wang, and Z. Zhang, J. Appl. Phys. **117**, 093907 (2015).
[43] A. Grutter, F. Wong, E. Arenholz, M. Liberati, A. Vailionis, and Y. Suzuki, Appl. Phys. Lett. **96**, 082509 (2010).
[44] R. Gunnarsson, Phys. Rev. B **85**, 235409 (2012).
[45] G. Herranz, B. Martinez, J. Fontcuberta, F. Sánchez, C. Ferrater, M. García-Cuenca, and M. Varela, Phys. Rev. B

67, 174423 (2003).
[46] J. Liu, S. Okamoto, M. Van Veenendaal, M. Kareev, B. Gray, P. Ryan, J. Freeland, and J. Chakhalian, Phys. Rev. B **83**, 161102 (2011).
[47] H. T. Yi, B. Gao, W. Xie, S.-W. Cheong, and V. Podzorov, Sci. Rep. **4**, 6604 (2014).
[48] X. Shen, X. Qiu, D. Su, S. Zhou, A. Li, and D. Wu, J. Appl. Phys. **117**, 015307 (2015).
[49] G. Herranz, F. Snchez, J. Fontcuberta, V. Laukhin, J. Galibert, M. Garca-Cuenca, C. Ferrater, and M. Varela, Phys. Rev. B **72**, 014457 (2005).
[50] S. Pang, Appl. Microsc. **47**, 187 (2017).
[51] L. Si, O. Janson, G. Li, Z. Zhong, Z. Liao, G. Koster, and K. Held, Phys. Rev. Lett. **119**, 026402 (2017).
[52] Y. Kumar, R. Choudhary, A. P. Singh, G. Anjum, and R. Kumar, J. Appl. Phys. **108**, 083706 (2010).
[53] L. Maritato, C. Adamo, C. Barone, G. De Luca, A. Galdi, P. Orgiani, and A. Y. Petrov, Phys. Rev. B **73**, 094456 (2006).
[54] A. Enders, R. Skomski, and J. Honolka, J. Phys. Condens. Matter. **22**, 433001 (2010).
[55] M. Ziese, Phys. Rev. B **68**, 132411 (2003).
[56] B. Li, H. Zhu, Q. Liu, Z. Liu, and Y. Zhang, J. Magn. Magn. Mater **366**, 50 (2014).
[57] A. Kostopoulou, E. Kymakis, and E. Stratakis, J. Mater. Chem. A **6**, 9765 (2018).
[58] W. Zhang, G. E. Eperon and H. J. Snaith, Nat. Energy **1**, 16048 (2016).
[59] X. Li, Y. Wu, S. Zhang, B. Cai, Y. Gu, J. Song, H. Zeng, Adv. Funct. Mater. **26**, 2435 (2016).
[60] Q. Zhang, S. Thota, F. Guillou, P. Padhan, V. Hardy, A. Wahl and W. Prellier, J. Phys. Condens. Matter **23**, 052201 (R) (2011).
[61] S. N. Jammalamadaka, J. Vanacken, and V. V. Moshchalkov, Appl. Phys. Lett. **105**, 033505 (2014).
[62] M. Ziese, I. Vrejoiu and D. Hesse, Appl. Phys. Lett. **97**, 052504 (2010).
[63] Y. Shiomi, Y. Handa, T. Kikkawa and E. Saitoh, Appl. Phys. Lett. **106**, 232403 (2015).
[64] M. Ziese, I. Vrejoiu, E. Pippel, P. Esquinazi, D. Hesse, C. Etz, J. Henk, A. Ernst, I. V. Maznichenko, W. Hergert, and I. Mertig, Phys. Rev. Lett. **104**, 167203 (2010).
[65] Y. Li, E. Choi, S.-I. Kim, S.-H. Baek, S.-Y. Park, Y. Jo, and J. Seo, AIP Adv. **7**, 085224 (2017).
[66] R. Scherwitzl, S. Gariglio, M. Gabay, P. Zubko, M. Gibert, and J.-M. Triscone, Phys. Rev. Lett. **106**, 246403 (2011).
[67] H. Wei, J. L. Barzola-Quiquia, C. Yang, C. Patzig, T. Höche, P. Esquinazi, M. Grundmann, and M. Lorenz, Appl. Phys. Lett. **110**, 102403 (2017).
[68] K. De and S. Das, B. MATER. SCI. **39**, 293 (2016).
[69] K. De, S. Majumdar, and S. Giri, J. Magn. Magn. Mater. **322**, 337 (2010).
[70] J. Zhang, Y. Xu, S. Cao, G. Cao, Y. Zhang, and C. Jing, Phys. Rev. B **72**, 054410 (2005).
[71] I. Mansuri and D. Varshney, J. Alloys Compd. **513**, 256 (2012).
[72] J. H. Cho, Q. X. Jia, X. D. Wu, S. R. Foltyn, and M. P. Maley, Phys. Rev. B **54**, 37 (1996).
[73] Y. Xu, J. Zhang, G. Cao, C. Jing, and S. Cao, Phys. Rev. B **73**, 224410 (2006).
[74] A. N. Pasupathy, R. C. Bialczak, J. Martinek, J. E. Grose, L. A. Donev, P. L. McEuen, and D. C. Ralph, Science **306**, 86 (2004).
[75] J. Kroha, arXiv preprint arXiv:1710.00192 (2017).
[76] H. Rostami, A. G. Moghaddam, and R. Asgari, J. Phys. Condens. Matter. **28**, 505002 (2016).
[77] P. Kharel, R. Skomski, P. Lukashev, R. Sabirianov, and D. J. Sellmyer, Phys. Rev. B **84**, 014431 (2011).
[78] P. A. Lee and T. V. Ramakrishnan, Rev. Mod. Phys. **57**, 287 (1985).
[79] S. Y. Li, L. Taillefer, D. G. Hawthorn, M. A. Tanatar, J. Paglione, M. Sutherland, R. W. Hill, C. H. Wang, and X. H. Chen, Phys. Rev. Lett. **93**, 056401 (2004).
[80] P. A. Lee and T. V. Ramakrishnan, Phys. Rev. B **26**, 4009 (1982).
[81] H. Boschker, M. Huijben, A. Vailionis, J. Verbeeck, S. van Aert, M. Luysberg, S. Bals, G. van Tendeloo, E. P. Houwman, G. Koster, J. Phys. D: Appl. Phys. **44**, 205001 (2001).
[82] A. Bhattacharya, S. May, S. Te Velthuis, M. Warusawithana, X. Zhai, B. Jiang, J.-M. Zuo, M. Fitzsimmons, S. Bader, and J. Eckstein, Phys. Rev. Lett. **100**, 257203 (2008).
[83] G. Zhou, C. Song, Y. Bai, Z. Quan, F. Jiang, W. Liu, Y. Xu, S. S. Dhesi, and X. Xu, ACS Appl. Mater. & interfaces **9**, 3156 (2017).
[84] S. May, T. Santos, and A. Bhattacharya, Phys. Rev. B **79**, 115127 (2009).
[85] M. Kawai, S. Inoue, M. Mizumaki, N. Kawamura, N. Ichikawa, and Y. Shimakawa, Appl. Phys. Lett. **94**, 082102 (2009).
[86] S. Y. Savrasov and D. Y. Savrasov, Phys. Rev. B **54**, 16487 (1996).
[87] M. Schultz, S. Levy, J. W. Reiner and L. Klein, Phys. Rev. B **79**, 125444 (2009).
[88] G. Bergman, Phys. Rev. Lett. **48**, 1046 (1982).
[89] C. Kittel, Phys. Rev. **73**, 155 (1948).
[90] V. Flovik, F. Maci, S. Lendnez, J. M. Hernndez, I. Hallsteinsen, T. Tybell, and E. Wahlstrm, J. Magn. Magn. Mater. **420**, 280 (2016).
[91] L. Steren, M. Sirena, and J. Guimpel, J. Appl. Phys. **87**, 6755 (2000).
[92] K. Zakeri, J. Lindner, I. Barsukov, R. Meckenstock, M. Farle, U. Von Hrsten, H. Wende, W. Keune, J. Rocker, S. Kalarickal, et al., Phys. Rev. B **76**, 104416 (2007).
[93] G. Woltersdorf and B. Heinrich, Phys. Rev. B **69**, 184417 (2004).
[94] A. Ghosh, J. Sierra, S. Auffret, U. Ebels, and W. Bailey, App. Phys. Lett. **98**, 052508 (2011).
[95] G. Luo, M. Belmeguenai, Y. Roussign, C. Chang, J. Lin, and S. Chrif, AIP Adv. **5**, 097148 (2015).
[96] G. Luo, C. Chang, and J. Lin, IEEE Trans. Magn. **49**, 4371 (2013).
[97] G. Luo, J. Lin, W.-C. Chiang, and C.-R. Chang, Sci. Rep. **7**, 6612 (2017)